PHOTONICS Research

Intracavity biosensor based on the Nd:YAG waveguide laser: tumor cells and dextrose solutions

Guanhua Li,[1] Huiyuan Li,[2] Rumei Gong,[3] Yang Tan,[4,*] Javier Rodríguez Vázquez de Aldana,[5] Yuping Sun,[3] and Feng Chen[4]

[1]Department of Respiration, Jinan Central Hospital Affiliated to Shandong University, Jinan, Shandong 250013, China
[2]Department of Ophthalmology, Jinan Central Hospital Affiliated to Shandong University, Jinan, Shandong 250013, China
[3]Department of Oncology, Jinan Central Hospital Affiliated to Shandong University, Jinan, Shandong 250013, China
[4]School of Physics, State Key Laboratory of Crystal Materials, Shandong University, Jinan 250100, China
[5]Departamento Física Aplicada, Facultad Ciencias, Universidad de Salamanca, Salamanca 37008, Spain
*Corresponding author: tanyang@sdu.edu.cn

Received 17 August 2017; revised 24 October 2017; accepted 26 October 2017; posted 27 October 2017 (Doc. ID 305016); published 17 November 2017

This work demonstrates the Nd:YAG waveguide laser as an efficient platform for the bio-sensing of dextrose solutions and tumor cells. The waveguide was fabricated in an Nd:YAG crystal with the cooperation of ultrafast laser writing and ion irradiation. The laser oscillation in the Nd:YAG waveguide is ultrasensitive to the external environment of the waveguide. Even a weak disturbance leads to a large variation of the output power of the laser. According to this feature, an Nd:YAG waveguide coated with graphene and WSe_2 layers is used as substrate for the microfluidic channel. When the microflow crosses the Nd:YAG waveguide, the laser oscillation in the waveguide is disturbed and induces fluctuation of the output laser. According to the fluctuation, the microflow is detected with a sensitivity of 10 mW/RIU.

OCIS codes: (230.7380) Waveguides, channeled; (140.0140) Lasers and laser optics; (280.3420) Laser sensors.

https://doi.org/10.1364/PRJ.5.000728

1. INTRODUCTION

Monitoring blood dextrose and cells is significant for medical diagnosis. Especially for first-aid, fast, precise, and portable (small) bio-detection is imperative [1,2]. For this purpose, microfluidic flow cytometry is developed for accurate detection of cells and solutions, which exhibits distinct advantages, including dynamic cell manipulation, isolation, and repeatability usage [3,4]. The sensing element with high sensitivity is the key component for microfluidic flow cytometry. Up to now, various technologies have been presented for optical flow sensing of a single cell, including flow cytometers and optofluidic circuits [5,6]. These technologies distinguish cells depending on the blocking or absorption of the detecting light, which is induced by the cell. For example, in the microfluidic channel, the cell crossing the 2D material changes the optical absorption of 2D materials [7–9]. Via the variation of the optical absorption (or the power of the detecting light), the solution and cells can be detected. For accurate detection, there is continuous motivation to amplify the fluctuation of the optical signal and further improve the sensitivity of the sensing element for a single cell.

The solid-state laser is ultrasensitive to the optical loss in the resonant cavity. Even a slight variation of the optical loss will trigger a large change of the power of the output laser. It seems the solid-state laser system may be used as a potential candidate for the amplifier of the variation of the loss induced by optical absorption. Recently, the fast development of the waveguide laser makes this proposal achievable. The waveguide laser is a laser system using the waveguide as the resonant cavity and the gain medium [10,11]. The dimension of the waveguide is small (cross-sectional area less than a hundred square micrometers, length around several millimeters), which is suitable for the combination with 2D materials [12,13] and the microfluidic channel [14,15]. It has been reported that the 2D materials coated on the surface of the waveguide can be used as the saturable absorber for the Q-switched laser emission [12,13]. Besides, the waveguide combined with the 2D materials can also be used for the sensing of the microflow in the microfluidic channel [14–16].

In this work, a highly sensitive biosensor is based on 2D materials and the waveguide laser. The graphene and WSe_2 layers were placed between the microfluidic channel and the waveguide laser, which work as both the sensing medium for the microstreaming and the absorber in the waveguide laser. We will show that the fluctuation of the optical absorption of graphene and WSe_2 is amplified by the laser oscillation process

in the waveguide, which provides high sensing of the live cell and the dextrose solution. Utilizing this device, the size of the cell is quickly distinguished, and the concentration of the dextrose solution is detected.

2. DESIGN AND METHODS

Figure 1(a) shows a diagram of the biosensor. The waveguides, with a length of 9 mm, were fabricated in the Nd:YAG crystal by the cooperation of the ultrafast laser writing and the ion irradiation. All the waveguides used in this work were fabricated under the same condition. Detailed information of the waveguide fabrication is reported in Ref. [17]. The heterostructure (G/W) consisted by graphene and WSe_2 monolayer is chosen as the absorber, due to the ultrafast optical response and the high optical absorption [18]. Graphene and WSe_2 were produced by the chemical vapor deposition and transferred onto the surface of the Nd:YAG waveguide. Figure 1(b) shows the high-resolution transmission electron microscopy (HRTEM) image of G/W heterostructure. Due to the lattice mismatching of graphene and WSe_2, the lattice of heterostructure displays a Moiré pattern. A polydimethylsiloxane (PDMS) microfluidic channel (purchased from Wenhao Co., Ltd.) was coated onto the G/W heterostructure [Figs. 1(c) and 1(d)]. The channel has a width of 100 μm and thickness of 50 μm.

This biosensor operates in two modes: so-called passive and active biosensor. The passive biosensor experiment is to provide a baseline for a standard single-pass absorption detection to compare with the multipass laser resonance detection. 1) The passive biosensor uses a continuous-wave laser (wavelength: 1064 nm; power: 10 mW) as the detecting light, and the information of the microflow is detected via the fluctuation of the output light. During the experiments, an off-chip laser is coupled into the waveguide through a spherical convex lens (focus length of 25 mm). And the output light is collected by a long work distance microscope objective (MO, 20×, N.A. = 0.4). 2) The active biosensor generates the laser oscillation at 1064 nm in the Nd:YAG waveguide, and detects the microflow by the fluctuation of the waveguide laser emission at the wavelength of 1064 nm. During the experiments, a polarized light beam at a wavelength of 810 nm from a tunable CW Ti:Sapphire laser (Coherent MBR 110) is coupled into the waveguide as the pumping laser. The output laser at 1064 nm from the waveguide is collected by the same microscope objective as the one used in passive biosensor.

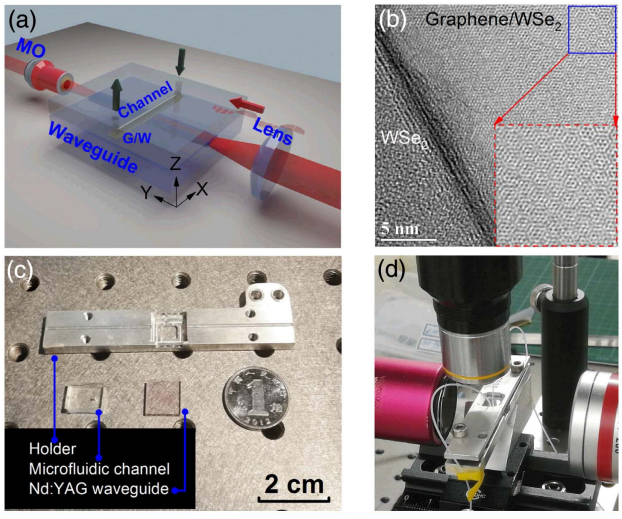

Fig. 1. (a) Diagram of the biosensor. (b) HRTEM image of G/W heterostructure. Graphene on the top and WSe_2 monolayer on the bottom. (c) Photograph of the microfluidic channel, Nd:YAG waveguide, and holder. (d) Photograph of the assembled biosensor.

3. RESULTS AND DISCUSSION

A. Passive Biosensor

Figure 2(a) shows the refractive index distribution on the longitudinal section of the Nd:YAG waveguide, which has a step-like shape. The propagation mode of the guided light at the wavelength of 1064 nm is also displayed in Fig. 2(a). The intensity of the light was concentrated near the surface, and the evanescent field of the guided light has an overlap with the G/W heterostructure with the length of 120 μm. Through the interaction with heterostructure, the guided light is absorbed by the heterostructure. The propagation loss of the waveguide is detected with the different polarization of guided light at the wavelength of 1064 nm. As shown in Fig. 2(b), without the heterostructure (blue dots), the waveguide with a length of 9 mm has a constant propagation loss of 0.4 dB. With the heterostructure (red dots), the loss has a maximum value of 1 dB at the *s* polarization (parallel to the waveguide surface) and a minimum value of 0.45 dB at the *p* polarization (vertical to the waveguide surface). Considering the length of the G/W heterostructure, the absorption due to the G/W is 5 dB/mm [(1–0.4 dB)/120 μm] and 0.4 dB/mm [(0.45–0.4 dB)/120 μm], corresponding to *s* and *p* polarizations. It demonstrates the G/W heterostructure has polarization-dependent absorption.

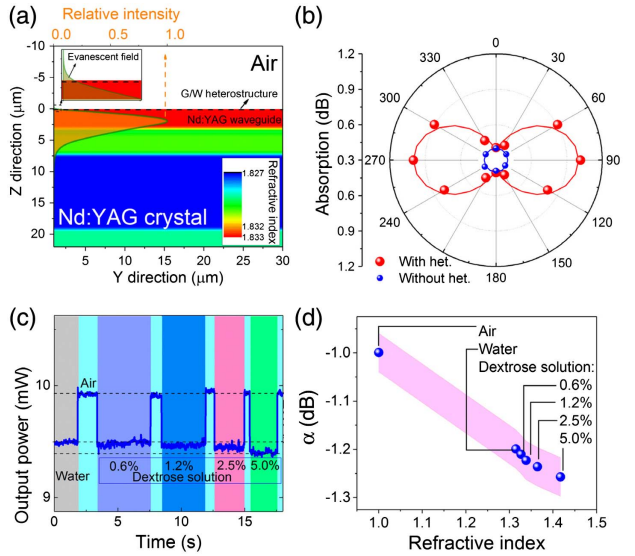

Fig. 2. (a) Refractive index distribution of the Nd:YAG waveguide and the propagation mode of the guided light at the wavelength of 1064 nm. (b) Polar image of the output light power along with the polarization variation. Wavelength of the detecting light is 1064 nm. (c) Real-time signal of different concentrations of dextrose solution. (d) Absorption coefficient corresponding to air, water, and dextrose solution.

In the following work, the light with s polarization is used as the detecting light.

The refractive index of the solution in the channel changes the optical absorption of the waveguide. When the solution crosses the waveguide surface, the intensity of the evanescent field is changed, leading to the variation of the absorption of the heterostructure. As a result, the microflow can be detected by the fluctuation of the power of the guided light in the waveguide [9,16]. Based on this biosensor, we used a continuous laser with the power of 10 mW at 1064 nm to detect the refractive index of the air, water, and dextrose solution. As shown in Fig. 2(c), there is an obvious fluctuation of the output power with the switching of air in the liquid, corresponding to the absorption coefficient of 0.9992 dB/cm (air) and 1.1991 dB/cm (water). For the dextrose solution with different concentrations, the absorption coefficient was slightly tuned between 1.210 dB/cm (0.6%) and 1.257 dB/cm (5%) in Fig. 2(d), which has a comparable change with the noise leading to a minimum concentration resolution of 0.5% (~2.5 mmol/L). This resolution is much lower than the resolution (~0.1 mmol/L) of the household blood glucose detectors.

B. Characteristic of the Nd:YAG Waveguide Laser

The laser oscillation in the Nd:YAG waveguide was excited by a continuous 810 nm laser. Figure 3(a) shows the spectrum and the near-field modal profile of the output laser at the wavelength of 1064 nm. The performance of the Nd:YAG waveguide laser is sensitive to the loss of the waveguide. To discuss the relationship of the laser performance and the loss, the loss of the Nd:YAG waveguide was artificially changed from 0.45 to 1.5 dB, via changing the overlay length (L) of the G/W heterostructure. As displayed in Fig. 3(b), there is great change of the threshold (P_{th}), slope efficiency (Φ), and output power of the Nd:YAG waveguide laser, along with the variation of the loss. With the increasing of the loss, P_{th} was increased from 26 to 84 mW [Fig. 3(c)], and Φ [Fig. 3(d)] was rapidly decreased from 63% to 4.5%, leading to a dramatic change of the maximum output power [Fig. 3(e)] from 50.4 to 0.4 mW.

As a four-level system, the relationship of the loss (α) and P_{th}/Φ of the Nd:YAG waveguide laser can be expressed as equations below [19]:

$$P_{\text{th}} = \frac{hcA_{\text{eff}}}{2\eta\sigma_e\tau\lambda_p}\delta = C_1\delta, \tag{1}$$

$$\Phi = \frac{\eta(T_1 + T_2)\lambda_P}{\lambda_L}\frac{1}{\delta} = C_2\frac{1}{\delta}, \tag{2}$$

$$\delta = 2\alpha L - \ln[(1 - T_1) \times (1 - T_2)], \tag{3}$$

where P_{th} is the laser threshold; h is the Planck's constant; c is the light velocity in the vacuum; λ_L and λ_P are the wavelengths of the laser and pump beams, respectively; σ_e is the stimulated emission cross section of Nd:YAG crystal; τ is the fluorescence lifetime; A_{eff} is the effective pump area; η is the fraction of absorbed photons that contribute to the population of the ${}^4F_{3/2}$ metastable state; T_1, T_2 are the transmittance of the end-faces; δ is the round-trip cavity loss.

As some parameters in Eqs. (1) and (2) are invariable, these equations are further simplified via introducing constants of C_1 and C_2. The value of C_1 and C_2 are obtained via fitting the measured results in Figs. 3(c)–3(e). Based on Eqs. (1)–(3), the maximum output power of the waveguide laser can be expressed as follows:

$$\begin{aligned} P_{\text{out}} &= \Phi(P_{\text{pump}} - P_{\text{th}}) = C_2\frac{1}{\delta}(P_{\text{pump}} - C_1\delta) \\ &= C_2\frac{1}{2\alpha L - \ln[(1 - T_1) \times (1 - T_2)]}P_{\text{pump}} - C_2C_1. \end{aligned} \tag{4}$$

To obtain the slewing rate of P_{out}, the partial derivative of P_{th} is taken with respect to α in Eq. (4). With the P_{pump} of 100 mW (at the wavelength of 810 nm), the maximum power of the Nd:YAG waveguide laser is 50.4 mW (at the wavelength of 1064 nm), and the calculated change of P_{out} per 0.01 dB (red line) is shown in Fig. 3(f). It seems the slewing rate has an exponential change along with α, and P_{out} has a higher sensitivity at the low loss. For our biosensor ($\alpha = 1$ dB), the slewing rate is ~0.52 mW per 0.01 dB [green line in Fig. 3(f)].

With the same conditions used in the passive biosensor, the slewing rate of the output laser per 0.01 dB (blue line) is also displayed in Fig. 3(f). In this situation, the variation of the output laser is only decided by $\Delta\alpha$. Compared with the active biosensor, the slewing rate is much lower in the passive

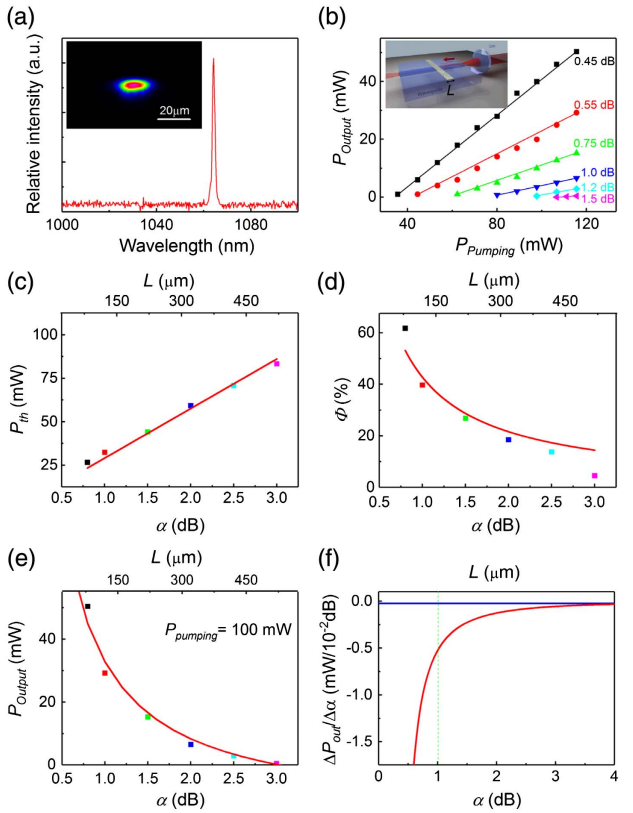

Fig. 3. (a) Emission spectrum of the output laser. Inset is the measured near-field modal profile of the emitted laser from the Nd:YAG waveguide. (b) Output power of the Nd:YAG waveguide as a function of the pumping power. Variations of (c) P_{th}, (d) Φ, and (e) P_{out}. (f) Calculated variations of P_{out} per 0.01 dB in the active (red line) and passive (blue line) biosensor.

biosensor. It demonstrates the difference of the absorption as amplified through the laser oscillation process.

C. Active Biosensor

The active biosensor (length of G/W 120 μm) is used to detect the same liquid displayed in Fig. 2(c). As shown in Fig. 4(a), there is a larger difference of the output power with the different liquid. For the conversion of the water and air, the maximum variation of the power is ~2.47 mW, which is much higher than the passive biosensor (~0.45 mW). Besides, the dextrose solution with different concentration (0.6%–5%) can be clearly distinguished. To compare the efficiency of the passive and active biosensor, the output power of detecting light is listed corresponding to the refractive index of the different liquid in Fig. 4(b). The sensitivity of the active and passive biosensor is 10 and 1.4 mW/RIU, respectively. It demonstrates that the fluctuation of the optical intensity is amplified by the laser oscillation in the waveguide, leading to higher sensitivity of the biosensor.

As reported in Ref. [9], the microsphere in the microflow changes the effective refractive index of the solution depending on the diameter of the microsphere; therefore, the refractive index sensing can also be used to sense the diameter of the microspheres. In this work, the active biosensor was used to distinguish the tumor cell and the PMMA ball. The tumor cell and PMMA ball have a diameter of ~20 μm [Fig. 5(a)] and ~10 μm, respectively. When a tumor cell or PMMA ball passes the waveguide laser through the microfluidic channel, the effective refractive index is increased, which leads to the increasing of the evanescent field. As a result, the power of the output laser has a rapid drop. The power of the output laser is detected by an ultrafast photoelectric probe and displayed on an oscilloscope (MSO/DPO5000B). As shown in Fig. 5(b), sharp dips were observed when an object crossing the waveguide laser. However, the intensity of dips was different, which depends on the types of objects (PMMA ball or tumor cell) [Figs. 5(b) and 5(c)]. Utilizing this feature, the tumor cell can be distinguished from the mixed solution of PMMA balls and tumor cells.

Figure 5(d) displays the real-time signal of the mixed solution of PMMA balls and tumor cells. Obviously, there are two different dips with the distinguished intensity. Through the counting of dips with different intensity, the concentration and type of the cell or ball in the solution could be obtained.

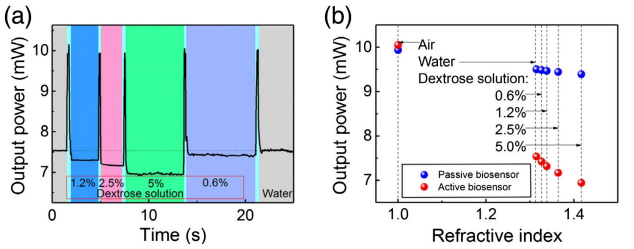

Fig. 4. (a) Real-time signal of different concentrations of dextrose solution in the active biosensor. (b) Output power of detecting light corresponding to the refractive index of the different liquid.

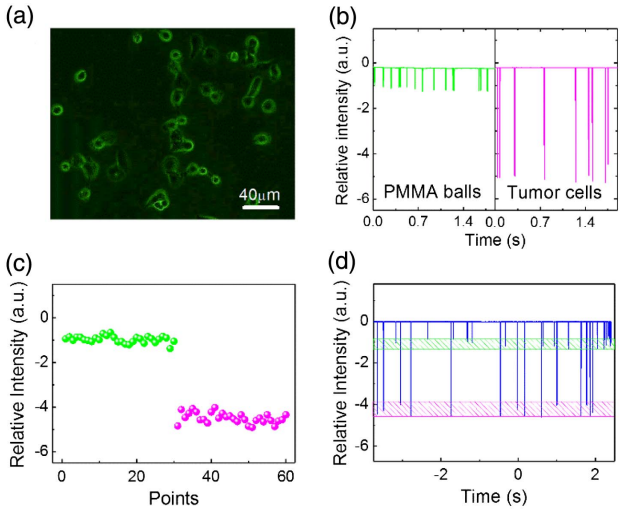

Fig. 5. (a) Microphotograph of the tumor cells. (b) Real-time signal of the solution of PMMA balls and tumor cells, respectively. (c) Repeatability of the active biosensor measurement. (d) Real-time signal of the mixed solution of PMMA balls and tumor cells.

4. CONCLUSION

We demonstrate the waveguide laser as an efficient platform for biosensing. The biosensor was constructed by Nd:YAG waveguide, G/W heterostructure, and a microfluidic channel. The microflow in the channel tuned the optical absorption of the G/W heterostructure, which is amplified by the laser oscillation in the Nd:YAG waveguide. The sensitivity of this biosensor is 10 mW/RIU. Based on this biosensor, we distinguished the concentration of the dextrose solution and tumor cells. This work paves a novel way for the live cell detection on a chip.

Funding. National Natural Science Foundation of China (NSFC) (11535008, 11775136); Young Scholars Program of Shandong University (SDU) (2015WLJH20).

Acknowledgment. Y. T. acknowledges the financial support from the Young Scholars Program of Shandong University.

REFERENCES

1. A. B. Chinen, C. M. Guan, J. R. Ferrer, J. R. Ferrer, S. N. Barnaby, T. J. Merkel, and C. A. Mirkin, "Nanoparticle probes for the detection of cancer biomarkers, cells, and tissues by fluorescence," Chem. Rev. **115**, 10530–10574 (2015).
2. V. Backman, M. B. Wallace, L. T. Perelman, J. T. Arendt, R. Gurjar, M. G. Müller, Q. Zhang, G. Zonios, E. Kline, T. McGillican, S. Shapshay, T. Valdez, K. Badizadegan, J. M. Crawford, M. Fitzmaurice, S. Kabani, H. S. Levin, M. Seiler, R. R. Dasari, I. Itzkan, J. Van Dam, and M. S. Feld, "Detection of preinvasive cancer cells," Nature **406**, 35–36 (2000).
3. T. D. Chung and H. C. Kim, "Recent advances in miniaturized microfluidic flow cytometry for clinical use," Electrophoresis **28**, 4511–4520 (2007).
4. D. Huh, W. Gu, Y. Kamotani, J. B. Grotberg, and S. Takayama, "Microfluidics for flow cytometric analysis of cells and particles," Physiol. Meas. **26**, R73–R98 (2005).
5. M. Kim, D. J. Hwang, H. Jeon, K. Hiromatsu, and C. P. Grigoropoulos, "Single cell detection using a glass-based optofluidic device fabricated by femtosecond laser pulses," Lab Chip **9**, 311–318 (2009).

6. Y. C. Tung, M. Zhang, C. T. Lin, K. Kurabayashi, and S. J. Skerlos, "PDMS-based opto-fluidic micro flow cytometer with two-color, multi-angle fluorescence detection capability using PIN photodiodes," Sens. Actuators B **98**, 356–367 (2004).
7. P. K. Ang, A. Li, M. Jaiswal, Y. Wang, H. W. Hou, J. T. L. Thong, C. T. Lim, and K. P. Loh, "Flow sensing of single cell by graphene transistor in a microfluidic channel," Nano Lett. **11**, 5240–5246 (2011).
8. S. Y. Yang, S. K. Hsiung, Y. C. Hung, C. M. Chang, T.-L. Liao, and G.-B. Lee, "A cell counting/sorting system incorporated with a microfabricated flow cytometer chip," Meas. Sci. Technol. **17**, 2001–2009 (2006).
9. F. Xing, G. X. Meng, Q. Zhang, L. T. Pan, P. Wang, Z. B. Liu, W. S. Jiang, Y. Chen, and J. G. Tian, "Ultrasensitive flow sensing of a single cell using graphene-based optical sensors," Nano Lett. **14**, 3563–3569 (2014).
10. C. Grivas, "Optically pumped planar waveguide lasers, part I: fundamentals and fabrication techniques," Prog. Quantum Electron. **35**, 159–239 (2011).
11. F. Chen and J. R. V. de Aldana, "Optical waveguides in crystalline dielectric materials produced by femtosecond—laser micromachining," Laser Photon. Rev. **8**, 251–275 (2014).
12. Y. Tan, C. Cheng, S. Akhmadaliev, S. Zhou, and F. Chen, "Nd:YAG waveguide laser Q-switched by evanescent-field interaction with graphene," Opt. Express **22**, 9101–9106 (2014).
13. Y. Tan, S. Akhmadaliev, S. Zhou, S. Sun, and F. Chen, "Guided continuous-wave and graphene-based Q-switched lasers in carbon ion irradiated Nd:YAG ceramic channel waveguide," Opt. Express **22**, 3572–3577 (2014).
14. R. Osellame, V. Maselli, R. M. Vazquez, R. Ramponi, and G. Cerullo, "Integration of optical waveguides and microfluidic channels both fabricated by femtosecond laser irradiation," Appl. Phys. Lett. **90**, 231118 (2007).
15. V. Maselli, J. R. Grenier, and S. Ho, "Femtosecond laser written optofluidic sensor: Bragg grating waveguide evanescent probing of microfluidic channel," Opt. Express **17**, 11719–11729 (2009).
16. Y. Tan, R. He, C. Cheng, D. Wang, Y. Chen, and F. Chen, "Polarization-dependent optical absorption of MoS_2 for refractive index sensing," Sci. Rep. **4**, 7523 (2014).
17. J. Lv, Z. Shang, Y. Tan, J. R. V. de Aldana, and F. Chen, "Cladding-like waveguide fabricated by cooperation of ultrafast laser writing and ion irradiation: characterization and laser generation," Opt. Express **25**, 19603–19608 (2017).
18. Y. Tan, X. Liu, Z. He, Y. Liu, M. Zhao, H. Zhang, and F. Chen, "Tuning of interlayer coupling in large-area graphene/WSe_2 van der Waals heterostructure via ion irradiation: optical evidences and photonic applications," ACS Photon. **4**, 1531–1538 (2017).
19. E. Lallier, J. P. Pocholle, M. Papuchon, M. P. De Micheli, M. J. Li, Q. He, D. B. Ostrowsky, C. Grezes-Besset, and E. Pelletier, "Nd: MgO: LiNbO/sub 3/channel waveguide laser devices," IEEE J. Quantum Electron. **27**, 618–625 (1991).